

The Nature of a Dusty Ring in Virgo

Noah Brosch & Elchanan Almoznino

The Wise Observatory and the School of Physics and Astronomy, Raymond and Beverly Sackler
Faculty of Exact Sciences, Tel Aviv University, Tel Aviv 69978, Israel

Bogdan Wszołek¹ & Konrad Rudnicki

Jagiellonian University Astronomical Observatory, ul. Orla 171, PL-30-244 Krakow, Poland

Received _____; accepted _____

¹Also at the Pedagogical University, ul. Armii Krajowej, PL-42-207 Częstochowa, Poland.

ABSTRACT

We detected a ring-like distribution of far-infrared emission in the direction of the center of the Virgo cluster. We studied this feature in the FIR, radio, and optical domains, and deduced that the dust within the feature reddens the galaxies in the direction of the Virgo cluster but does not affect stars within the Milky Way. This is likely to be a dusty feature in the foreground of the Virgo cluster, presumably in the galactic halo. The HI distribution follows the morphology of the FIR emission and shows peculiar kinematic behavior. We propose that a highly supersonic past collision between an HI cloud and the Galactic HI formed a shock that heated the interface gas to soft X-ray temperatures. HI remnants from the projectile and from the shocked Galactic HI rain down onto the disk as intermediate velocity gas.

Our finding emphasizes that extragalactic astronomy must consider the possibility of extinction by dust at high Galactic latitude and far from the Galactic plane, which may show structure on one-degree and smaller scales. This is particularly important for studies of the Virgo cluster, for example in the determination of the Hubble constant from Cepheids in cluster galaxies.

Subject headings: ISM: dust, extinction, stars, galaxies: clusters: individual: Virgo

1. Introduction

The nature of non-luminous matter that is not part of detected and catalogued galaxies remains unsolved by modern astrophysics. As mentioned in a recent thesis, low surface brightness (LSB) objects may prove to be the “icebergs” of the extragalactic world (de Blok 1997). Some searches for non-luminous matter have been successful, *e.g.*, the detection of a giant HI ring around the small group of galaxies in Leo centered on M96 (Schneider *et al.* 1983), extended HI emission in the M81 group (Lo & Sargent 1979), HI companions to dwarf galaxies (for $\sim 25\%$ of the cases: Taylor *et al.* 1996), and a large neutral hydrogen cloud in the southern outskirts of the Virgo cluster (HI 1225+01: Giovanelli & Haynes 1989).

Along with HI clouds, a few large LSB galaxies have been identified: Malin-1 (Bothun *et al.* 1987), F568-6 (Bothun *et al.* 1990), and 1226+0105 (Sprayberry *et al.* 1993). Their typical star formation rates are $\sim 0.1 \text{ M}_\odot/\text{yr}$ and the metallicities are $\sim 1/3$ solar. The HI rotation curves, measured by de Block *et al.* (1997) and by Pickering *et al.* (1997), indicate that their gaseous component is dynamically significant at all radii and that the galaxies are fully dark-matter dominated; their detected baryonic component is less than 4% of the total mass. This last conclusion is valid at least as long as we do not accept any of the more exotic theories of gravitation. The LSB galaxies lack bulges, bars, and nuclear activity, as well as CO or IR emission (*i.e.*, have no molecules or dust).

There have also been a few intriguing reports of presumably intergalactic dust clouds. A cloud with 0.5-1.2 mag of extinction was identified in Microscopium by Hoffmeister (1962). Three other similar objects were listed by Rudnicki (1986); they extinguish background objects by 0.57 to 1.2 mag. In all reports the main point of contention was the actual distance to the cloud, which could put it in extragalactic space but could also locate it in the halo of the Milky Way (MW). Sometimes, the argument for an extragalactic location was based on a comparison of the properties of objects whose distance could be estimated and which were located behind the cloud with those of similar objects clearly not within the cloud limits (*e.g.*, RR Lyrae stars; Murawski 1983).

The extragalactic nature is only fairly confidently established for the Abadi-Edmunds cloud at ~ 3 Mpc (Abadi & Edmunds 1978). HI 21 cm line emission was detected from this object, whereas in other cases it was not. However, in other cases far-infrared (FIR) emission was detected and could be identified (on morphological and positional criteria) with the obscuring clouds. FIR and HI emission were clearly detected in the case of the Okroy cloud (Wszolek *et al.* 1988a, 1989). FIR emission was only marginally detected from the Rudnicki-Baranowska cloud (Wszolek *et al.* 1988b). This indicates that the physical conditions in this kind of objects are far from being uniform. More such examples must be identified and their properties examined.

It is possible that the phenomenon of intergalactic hydrogen clouds could be related to the high-velocity cloud (HVC) complexes. These are HI structures whose radial velocities deviate by several 100 km s^{-1} from the conventional galactic rotation. A recent review of HVCs is by Wakker & van Woerden (1997). Their Table 2 lists a few cloud complexes at distances $\geq 25 \text{ kpc}$; some of these may not belong at all to the MW. IRAS searches for FIR emission of HVC were negative (*e.g.*, Wakker & Boulanger 1986), indicating that either the HVCs are dust-free or that their dust grains are much cooler than could be detected with IRAS. In this context we also mention the proposition by Blitz *et al.* (1999) that the HVCs make up the missing mass by being essentially dark halos with low velocity dispersions.

We report here results from a study of a diffuse ring-like FIR feature at high galactic latitude, which we interpret as “local”, *i.e.*, not extragalactic, despite first indications to the contrary. The region toward which this feature is located is the center of the Virgo cluster of galaxies. This part of the sky has been studied in exquisite detail, yet new studies always detect interesting features. For example, Katsiyannis *et al.* (1998) produced a very deep image of the central regions of the cluster from a combination of 13 deep Kodak TechPan films obtained with the UK Schmidt telescope. The image shows large variations in the brightness of the intra-cluster medium, with the brightest regions north of the cluster center. M87 is fairly central in the region of enhanced brightness, close to the upper left corner of the “very high contrast image” in their Fig. 6. Previous deep imaging of the central VC region (*e.g.*, Weil *et al.* 1997) revealed a diffuse extension

of (presumably stellar) material extending \sim 100 kpc to the SE of M87. Intergalactic red giant stars were apparently discovered near M87 by Ferguson *et al.* (1998). It is therefore relevant to search for, and to try and explain, any extended feature one may detect in the direction of the center of the cluster. In this context, we mention the study of Haikala *et al.* (1995) who examined the UV emission detected in the direction of a dust globule close to the North Galactic Pole, slightly north of the Virgo cluster (VC).

Any material that could produce extinction needs to be accounted for. To the best of our knowledge, nobody attempted to study the obscuration and FIR emission by ISM or IGM in the direction of a rich, nearby cluster of galaxies. This is particularly important for the VC, which serves as one of the key stones in the distance ladder leading up to the determination of the Hubble constant (*e.g.*, van den Bergh 1996). The HST Key Project on the Extragalactic Distance Scale, where the required accuracy of the determination of H_0 is 10%, could be affected significantly by unaccounted extinction. Until now, seven galaxies within 10° of the Virgo center have been observed for Cepheids in this context (Macri *et al.* 1999).

The plan of the paper is as follows: we first describe the FIR observations, which revealed the feature, and present confirmatory evidence of its reality. We then attempt to derive additional properties of the feature, which has an approximate ring shape, using data in the optical and radio domains. We show that the dust in the feature does not seem to affect the stars in the Milky Way but that it apparently reddens galaxies in the VC and beyond. The full data set is discussed in the last section of the paper, in which we also derive some properties of the dust grains in the feature.

2. Observational data

2.1. COBE/DIRBE

Far infrared (FIR) observations from the COBE satellite, specifically with the DIRBE instrument, reveal non-uniform FIR emission from the center of the VC. The DIRBE instrument mapped the entire sky at ten wavelength bands from 1.25 to $240\mu\text{m}$ and operated from November

1989 to December 1993 (cryo-cooling was available only for ten months, restricting the availability of the FIR channels). An important feature of DIRBE was that the measurements were performed against an internal calibrator source, with proper accounting for instrumental offsets and interplanetary FIR emission. For the present analysis we used the Annual Average Sky Maps (AASM: Hauser *et al.* 1997), which provide a single, ten-month averaged intensity value per pixel in each of the DIRBE bands. Note that the zodiacal light contribution was not subtracted from the DIRBE counts. This is because we do not estimate the zodiacal contribution to the FIR bands to be significant or to show features on the angular scales relevant here.

We conducted a number of studies of galaxies in the Virgo cluster in which we studied various photometric indices for entire objects as well as for localized regions in each galaxy (*e.g.*, Almoznino & Brosch 1998, Heller *et al.* 1998). The possibility that these programs could be affected by foreground dust imposed our selection of the Virgo Cluster as the initial target for combined FIR and other spectral band interpretations.

We detected a ring-like structure of FIR emission in COBE/DIRBE maps of the VC, which is centered approximately on M87. The ring is approximately centered on (1950) 12^h31^m ; $+13^\circ$ ($l=285^\circ.8$, $b=75^\circ$; J2000) and its diameter is $\sim 4^\circ$. The width of the FIR emission in the rim of the ring is $\sim 1^\circ$. The detection was made originally on the COBE/DIRBE maps, but the existence of the feature was established also on IRAS maps (see below). The M87 galaxy ($l \approx 282^\circ.5$, $b \approx +74^\circ.4$) is normally taken as the center of the Virgo Cluster (VC) and one could imagine scenarios by which some sort of FIR-emitting matter could be distributed around it. For this reason, we decided to follow the FIR detection of the feature, which we call here “the Virgo Ring” (VR), and investigate it further.

The detection was made on the AASM, which have noise levels of $3 \text{ } 10^{-3} \text{ MJy sr}^{-1}$ at $100\mu\text{m}$, 0.6 MJy sr^{-1} at $140\mu\text{m}$, and 0.3 MJy sr^{-1} at $240\mu\text{m}$ (Kashlinsky 1999). The ring is visible even by superficial inspection of these COBE/DIRBE gray scale maps. No traces of the ring can be seen on $60\mu\text{m}$ or shorter wavelength maps. To obtain detailed insight into the structure of the VR we produced isophotal maps at $\lambda=100$ and $240\mu\text{m}$ using the original $0^\circ.3$ square pixels, which

are shown as isophote plots in Figure 1. The $100\mu\text{m}$ map shows a region of depressed FIR flux where $F_{100} \approx 8.2 \text{ MJy sr}^{-1}$. This is surrounded by regions of enhanced FIR emission, which reach $F_{100} \approx 10 \text{ MJy sr}^{-1}$. The $240\mu\text{m}$ map indicates that the region of reduced FIR emission has $F_{240} \approx 3.7 \text{ MJy sr}^{-1}$ while the surrounding regions have $F_{240} \approx 5 \text{ MJy sr}^{-1}$. It is clear that (a) the DIRBE data indicate a region of low FIR emission surrounded by enhanced emission, and (b) the feature is real, because it appears on more than one DIRBE map. The lowest values of the FIR flux originate presumably from the zodiacal light that was not subtracted from the AASMs and from the cosmic FIR background. As both these components are much smoother than the feature we describe here, there is no need to model them in detail.

2.2. IRAS

The peculiar FIR features detected by COBE/DIRBE are confirmed by IRAS measurements. The IRAS mission mapped the sky in four wavelength bands from January 1983 to November 1983. The primary goal of the IRAS survey was the detection of point sources, but a catalog of extended sources has also been produced, as well as sky brightness images in each of the four bands with $2'$ pixels and $4'-6'$ resolution (Beichman *et al.* 1988).

IRAS 60 and $100\mu\text{m}$ Extended Emission Data in the $16^\circ.5 \times 16^\circ.5$ square fields no. 83 and 84 were used to confirm the existence of the ring and to exclude the possibility of instrumental artefacts produced by the COBE/DIRBE instrument. We created maps at these two spectral bands with a $4' \times 4'$ beam. The VR is clearly visible on the $100\mu\text{m}$ map shown in Fig. 1. A similar $100\mu\text{m}$ map based on IRAS observations, and where this feature is also visible, was reproduced already by Leggett *et al.* (1987) as their Plate 2. The enhanced IRAS resolution relative to COBE/DIRBE allows a good morphological evaluation of the FIR feature. In addition to the north-westerly extension of the FIR emission, along the IRAS scan direction, one sees an arc-like distribution of emission, which could be interpreted as forming an elliptical ring. Note that the feature is visible only on the $100\mu\text{m}$ map (shown in Figure 1) and is not seen on the $60\mu\text{m}$ map, or on those at even shorter wavelengths (not shown here).

Although the low resolution COBE/DIRBE maps seem to indicate that the FIR emission is arranged in a ring, with low FIR at the center and high emission on its perimeter, the higher resolution IRAS maps show that this is not the case. The FIR emission is distributed in an open configuration, with a region of low emission centered on $\sim 12^h 30^m$, $+13^\circ.2$. The FIR emission could best be described as a fork, or a two-arc shape limited to $\alpha=185^\circ - 189^\circ$. The eastern side of the feature shows a small region of enhanced FIR emission centered on $\alpha=185^\circ$ and $\delta=13^\circ.5$ that stands out over its surroundings and to which we refer as the “main blob” (MB).

2.3. Optical information: stars

The dust revealed by the FIR observations may (a) extinguish and (b) redden stars behind it. The first effect is a consequence of the “total extinction” property, whereas the second is the result of “wavelength-selective extinction”. The relative importance of the two effects is linked through the parameter $R = \frac{A_V}{E(B-V)}$, which is determined to first order by the size of the dust grains.

We tested two assumptions, one of extinction within the Milky Way (MW) that would affect some of the stars but not others, and a second that the VR is extragalactic and is located between the MW and the VC. In the second case it would affect the VC galaxies, but none of the MW stars.

For testing the possibility that the dust is “local” one requires a large number of stars with magnitudes and colors. These were extracted from the USNO-A2.0 catalog, which includes blue and red magnitudes for each star. The USNO-A2.0 catalog contains $>5 \cdot 10^8$ objects ($\sim 12,750$ per square degree) and is based on scans of the Palomar Sky Survey (PSS) plates produced with the Precision Measuring Machine (PMM). The catalog is an improvement over the version 1.0 both in astrometric accuracy and in photometric precision. The photometric accuracy is probably not better than ~ 0.15 mag, but the depth of the catalog is considerable, as it reaches 20-22 mag (color-dependent). It can, therefore, serve as a source of stellar objects with which one can test the assumption of foreground extinction.

We extracted objects in a number of $1^\circ \times 1^\circ$ regions from the USNO-A2.0 catalog. The extraction locations are listed in Table 1 and correspond to some FIR-bright regions (where we expect a higher density of extinguishing dust) or to some FIR-faint regions (which should be \sim transparent). We produced Wolf diagrams for each location, and show these in Figure 2. The Wolf diagrams plot the cumulative distribution of stellar magnitudes against magnitude, and the signature of total extinction in such a plot is a step-like deviation, to fainter magnitudes of the cumulative star counts, from the pattern set by the brighter (and closer, on average) stars. The diagrams do not show such a step-like trend for regions in the direction of stronger FIR emission when compared with the behavior of the cumulative distribution in regions with lower FIR emission.

It is also possible to compare the measured behavior of the cumulative star counts with that “predicted” in absence of localized extinction effects by using a model for the stellar distribution in the Galaxy for the same Milky Way locations as sampled here. A very successful and intuitively simple stellar distribution model was produced by Bahcall & Soneira (1984) and is available on-line². We calculated predicted star counts for the locations of the extracted data from the USNO-A2.0 catalog using the version of the model retrieved in December 1998. The locations are listed in Table 1. We compared the predicted cumulative star counts with the actual star counts. The comparisons are shown in Figure 3 and show no significant deviations from the predicted behavior.

The exercises shown in Figs. 2 and 3 indicate that the stellar distributions are not influenced by the material producing the FIR emission. The conclusion is, therefore, that this material is either extremely nearby, so that all the stars are affected in the same manner, or that it is very distant, beyond the more distant stars listed in the USNO-A2.0 catalog.

²<http://www.sns.ias.edu/~jnb/Html/galaxy.html>

2.4. Optical information: galaxies

If the dust observed in the FIR does not affect stars in our galaxy, it may be located far from the MW and could affect only objects seen behind it. Testing the assumption of a dust cloud distant from the MW requires a sample of background objects with relatively high surface density, as well as brightness and color information. In the Virgo region, the “standard” extragalactic catalog has been for a number of years the Binggeli *et al.* (1985) Virgo Cluster Catalog (VCC). The VCC covers \sim 140 square degrees and contains 2096 galaxies. The surface density of galaxies is, therefore, \sim 15 galaxies/square degree, on average. While this may appear sufficient, the photometry is not adequate because the galaxy magnitudes in the VCC are eye estimates and may have significant deviations. In addition, no colors are available for most VCC galaxies. We decided therefore to rely on a more recent galaxy compilation, which reaches deeper in brightness and is thus denser than the VCC, has better photometry, and contains color information for the objects.

Currie & Young (1998, hereafter VPC) produced an extensive three-color photometric catalog of galaxies in the central regions of the VC. The catalog is based on COSMOS scans of one U plate, two B_J plates, and one R_C plate, all obtained with the UK Schmidt telescope. The plates were photometrically calibrated and objects were extracted automatically, with stars and galaxies separated by an automatic algorithm. The VPC provides an impartial survey of galaxies in the region of interest for the present study, which reaches to $B_J \approx 19$ mag, thus it is somewhat shallower but comparable in depth with the stars from the USNO-A2.0 catalog. The area covered by the VPC covers 23 square degrees and is centered on (1950) 12:26 +13:08. The average galaxy surface density is therefore 49 galaxies/square degree, considerably more than that of the VCC.

We attempted to detect total extinction effects on the VPC galaxies by limiting the analysis to regions with high FIR emission and comparing these with similar analyses in the direction of regions with lower FIR emission. Four parallelogram-shaped fields were selected, marked A, B, C, and D on Figure 4. Fields C and D are used to determine the nature of the galaxy population in the general region of the VR. Field A could also be used for this purpose, but we caution that a background cluster of galaxies (Abell 1552 at $z \approx 0.084$) is located in this field and thus region

A may not be representative. This galaxy cluster is presumably part of a background sheet-like complex, which includes also Abell 1526 at a very similar redshift. Field A was selected to offer insight on how the presence of background galaxies disturbs the results. The enhancements of the galaxy background may distort the Wolf diagrams of galaxies (Figure 5), and indeed some FIR enhancements could be in the direction of these galaxy clusters. However, searches for dust in clusters of galaxies have, so far, been negative (Maoz 1995). Thus, we may tentatively discount the FIR enhancements in the direction of background clusters of galaxies as chance superpositions. Field B is considered not to be affected by absorption/extinction and is in the direction of the low FIR emission of the VR.

Attempts to detect the presence of dust as a “total extinction” effect, which modifies the cumulative galaxy counts between the different regions, were not successful. The differences were not significant and indicate that if dust is present, it may cause at most a small amount of total extinction: $A_B \leq 0.5$ mag. We therefore checked for the presence of color-dependent extinction by studying the distribution of the $(U-R_C)$ color index in one square degree areas over the central part of the Virgo cluster. The data used for this test, and an extensive description of the method and results, are given in the Appendix to this paper. Here we emphasize that the results show that the galaxies in the direction of the Virgo Ring (VR) part with the lowest FIR emission appear slightly bluer than those in the direction of the two regions with higher FIR emission. The difference is significant to $\geq 95\%$. Interpreted as dust extinction, this difference in average $(U-R_C)$ color index indicates a possible wavelength-dependent extinction of $\Delta(U-R_C) \simeq 0.3$ mag between areas with high FIR emission and areas with less dust, *i.e.*, a total extinction $A_V \simeq 0.33$ for a typical Milky Way extinction law, although this was not checked here.

2.5. Radio information

Here we show that X-ray observations of the region indicate a two-component makeup for the hot gas, and that the morphology and kinematics of the HI are peculiar. Böhringer *et al.* (1995) mapped the X-ray emission from the immediate vicinity of M87; this is the region of interest of

the present study. Their findings show the presence of thermal X-ray emission from cooler gas than the intracluster medium. A ROSAT map of the general region, larger than the one analyzed in the 1995 paper, was presented by Böhringer *et al.* (1994) and shows a ridge of X-ray emission which approximately coincides with the FIR emission ridge to the west of M87. They mention, in particular, the sharp drop in X-ray intensity on the western side of M87. Böhringer *et al.* (1994) subtracted a model distribution of X-rays from M87 from the ROSAT map and derived a residual map (their Fig. 2) which shows the background cluster A1552 at 12:30+11:30 and a long filament, which is elongated \sim north-south at $\alpha \approx 12^h 30^m$ and from $\delta \approx +15$ to $+6$. This filament curves around M87 on its westerly side and seems to follow the contours of the $100\mu\text{m}$ emission.

It is tempting to speculate on a possible link between the X-ray and FIR emission presented above, but we caution that this may not be real. One possible factor affecting the morphology of X-ray emitting gas is the amount of foreground HI, which modifies mainly the low energy end of the X-ray spectrum. Shadows in the X-ray background caused by foreground HI clouds have been detected mainly in soft X-rays by *e.g.*, Egger & Aschenbach (1995). However, the feature detected in the ROSAT maps by Böhringer *et al.* (1994) is seen in the hard energy band (0.4–2.4 keV), and is thus difficult to attribute it to gas absorption.

EUVE observations of the Virgo cluster (VC) center (Lieu *et al.* 1996) show the presence of gas at $\sim 0.5 \cdot 10^6$ K near M87. This matter forms an additional component of the intra-cluster material (ICM) in Virgo, as follows from their analysis, and cannot be the same hot gas which is responsible for the X-ray emission detected by ROSAT. In order to confirm the existence of this second ICM component of the VC, Lieu *et al.* (1996) performed HI 21 cm observations with the 43-m Green Bank telescope (angular resolution $21'$). The region surveyed by them was centered on M87, had an extent of $2^\circ \times 1^\circ.6$, and the grid of HI measurements was spaced every $8' \simeq 1/3$ of a resolution element.

A comparison of the HI map of Lieu *et al.* (1996) with the FIR distributions (see Figure 1) demonstrates that the FIR emission follows the total HI column density. Although Lieu *et al.* do not mention the velocity range over which the Green Bank observations were performed, we

assumed these to be at ~ 0 km s $^{-1}$ because they are supposedly of “Galactic HI” origin. While some VC galaxies do have negative heliocentric velocities (c.f. Binggeli *et al.* 1985), they mostly concentrate at 1,000–2,000 km s $^{-1}$. For this reason, we think it likely that the HI detected by Lieu *et al.* (1996) does indeed belong to the MW and, by inference, so does the material producing the FIR emission. We note at this point that the center of the low N(HI) region, at 12:28+12:45 (1950) and only \sim half a degree away from M87, has $N(\text{HI}) \simeq 1.8 \text{ } 10^{20} \text{ atoms cm}^{-2}$. This is coincident with the low FIR emission region. The ridges with the higher N(HI) values correspond to enhanced FIR emission regions.

We produced N(HI) plots for the region using data from the Leiden-Dwingeloo HI survey (Hartmann & Burton 1997, LDS) in order to confirm the HI distribution measured by Lieu *et al.* (1996). The LDS was conducted with the 25-m radio telescope at Dwingeloo and the data we used cover the velocity range $-459 < v_{lsr} < +415$ km s $^{-1}$ with a resolution of 1.03 km s $^{-1}$. The 25-m radio telescope has a 36' half-power beam and the survey was performed with 0°.5 spacings. We used the file TOTAL_HI.FIT from the CD-ROM supplied with the printed atlas to extract the proper sky region. The data were transformed from Galactic to equatorial coordinates, accounting for the change of scale from one side of the image to the other. This was done by dividing each pixel value by its $\cos(b)$, to yield consistent units over the field. The HI total column density from the LDS is shown in Figure 6 together with the IRAS 100 μm map and confirms the general impression from the Lieu *et al.* (1996) map. The HI distribution has a region with lower N(HI) at the center of the Virgo Ring (VR) and ridges of higher HI emission on both sides of the VR.

We also produced position-velocity (PV) plots using the channel data from the LDS, limiting these to $l=276.0$, the galactic longitude of the HI peak which coincides with the main FIR emission blob in area A of Fig. 6 (the more intense of the FIR peaks), to the center of the VR ($l=283.0$), and to the second highest FIR peak at $l=290.5$. The PV plots are shown in Figure 7 and indicate that at the position of the VR there is a significant disturbance of the HI, with a strong extension to negative velocities appearing in the PV plots of the high-FIR region. The sheet-like HI distribution, which links HI at low latitudes with gas near the Galactic Pole and has

a slightly negative LSR velocity, appears disturbed at $b \approx 75^\circ$.

The velocity plot through the peak emission at $l=276.0$ at this latitude (Figure 8) shows three peaks separated by ~ 20 km s $^{-1}$. The strongest has the most negative velocity, approximately -30 km s $^{-1}$ and a FWHP of ~ 11 km s $^{-1}$. The weakest peak at this location is near $+4$ km s $^{-1}$ (LSR). The PV in the low FIR region at the center of the VR ($l=283^\circ$, $b \approx 75^\circ$) shows a single strong peak at ~ -7 km s $^{-1}$ (LSR), with a FWHP of 12.5 km s $^{-1}$ and a low shoulder extending to more negative velocities, down to the velocity of the strong peak at the location of the main blob (-30 km s $^{-1}$). The third PV, at ($l=290^\circ.5$, $b \approx 75^\circ$) is narrow with a FWHP of ~ 5 km s $^{-1}$ and is centered at -7 km s $^{-1}$ (LSR).

3. Discussion

We identified a ring-like feature of FIR emission at high galactic latitude, which is distant from the main body of the Galaxy and extinguishes light from galaxies in the central part of the Virgo cluster (VC). There is no way to establish a distance to the extinguishing cloud with the data we presented above, except to note that it is probably >1 kpc.

A nearby dust feature, observed by Haikala *et al.* (1995) in the far-UV, has been located at ~ 120 pc using the distribution of E_{b-y} color excesses. This dust clouddlet produces a visual extinction $A_V \leq 0.4$ mag and is located at ($l=251.1$, $b=+73.3$); this location is very similar to what we found for the Virgo Ring (VR) and may indicate that either our distance evaluation is wrong, or that the location technique of the Haikala *et al.* feature did not use a sufficient number of more distant stars.

Indications that the dust cloud cannot be a nearby feature originate mainly from the lack of influence on the distribution of stars. Supporting evidence to the same comes from the reddening study of Knude (1996). He used uvbyH β measurements of A3-G0 stars with $B \leq 11.5$ mag and $|b| > 70^\circ$ to determine the distribution of extinction. His results for E_{b-y} , broken by galactic latitude and by longitude quadrants, are of particular interest. The area of interest for our study

is located between the 3rd and 4th quadrants at $b \approx 75^\circ$; the reddening to this region is small, $E_{b-y} \leq 0.017$, which translates into $A_B \leq 0.095$. The stars studied by Knude (1996) are closer than 1.5 kpc (for main sequence A stars brighter than 11.5 mag), thus the color-dependent extinction of the VC galaxies we detected, which is equivalent to $A_B \approx 0.4$ mag, should be produced by material more distant than 1.5 kpc.

If the cloud would be in the VC itself, its physical size would be ~ 1.5 Mpc, very large indeed ! The issue of possible diffuse dust in clusters of galaxies has been studied by *e.g.*, Ferguson (1993). He concluded, from the lack of a difference between cluster and field galaxies in the correlation of the Mg_2 index and $(B-V)$, that dust is not present in the Virgo cluster (upper limit $E(B-V) < 0.06$ mag.). A similar conclusion for a large number of Abell clusters, based on the $(V-I)$ color indices of radio quasars seen in their background, was reached by Maoz (1995).

Not accounting for foreground dust may affect adversely some key observations. Our finding confirms the supposition of Zonn (1957) and Zonn & Stodolkiewicz (1958), that because of the patchy structure of the interstellar dust *it is not enough to correct for extinction assuming that the dust is localized in a narrow slab near the Galactic equator, but the detailed distribution of dust must be investigated to account properly for the extinction*. In particular, many observations of the Virgo cluster and of objects within (*e.g.*, the HST Cepheid Key Project: Graham *et al.* 1998, Macri *et al.* 1999) may carry significant errors because of improper extinction corrections.

In this section we estimate the dust temperature and dust-to-gas ratio. To evaluate the temperature of the dust in VR we subtracted from the map intensities the minimal value for the central part of the VR, near M87, in the 100 and $240\mu\text{m}$ COBE/DIRBE bands (8 and 3.5 MJy sr $^{-1}$ respectively). To determine the color temperature for the dust in the VR cloud we assumed that the dust particles are in thermal equilibrium and that the foreground galactic IR radiation and IR emission from all point sources in the region have been subtracted accurately. These assumptions may not be necessarily fulfilled in our case. The subtraction of the intensity of the inner part of the ring would be accurate only if the distribution of the foreground galactic radiation is fairly smooth; this is not the case even at high galactic latitudes. Some galactic

features may add non-negligible FIR contributions to the foreground. The radiation from very cold dust grains ($T \approx 3K$) could not be detected by the means used here. We could not rule out the possibility that transient heating of dust grains takes place, and that only occasional excitation by energetic photons or particles causes them to emit brief pulses of the radiation measured by COBE/DIRBE and IRAS.

With all these caveats in mind, we calculated the temperature of two regions with maximal FIR intensities within regions delimited by: α : 185° – 186° , δ : 13° – 14° (approximately the Main Blob=MB region) and α : 189° – 190° , δ : 12° – 13° (slightly off the secondary FIR peak). The temperature was calculated with the relation:

$$\log_{10}T = 1.30274 + 0.26266(\log_{10}R) + 0.04935(\log_{10}R)^2 \quad (1)$$

from Schlegel *et al.* (1998), where $R = \frac{I_{100}}{I_{240}}$ is the ratio of the FIR intensities in the COBE/DIRBE bands. The results are 22 and 20K for the first and the second region, respectively. These values can be accepted as upper limits for the dust temperature in VR due to both effects mentioned above. The temperatures do not differ significantly from those usually adopted for interstellar dust clouds and are at the high end of the range for the “warm” cirrus component (Lagache *et al.* 1998). The difference between the two regions, with the MB being “hotter” than the secondary FIR blob, is marginally significant, because the formal error in the derivation of temperatures is 1-2K.

A study of the optical depth effects of high latitude clouds (Chlewicki & Laureijs 1988) found that typically $\frac{I_{100}}{N(HI)} = 0.7$ MJy ster $^{-1}$ /10 20 atoms cm 2 . Deul & Burton (1990) studied the HI content and gas kinematics of seven cirrus clouds detected in the IRAS maps. They established that the FIR to HI ratio varies between 0.9 and 3.0 MJy ster $^{-1}$ /10 20 atoms cm $^{-2}$. The color temperature varies much less, between 0.20 and 0.27 for $\frac{I_{60}}{I_{100}}$. Unfortunately, we did not detect 60 μ m emission from the VR, thus a direct comparison with the color temperature derived by Deul & Burton (1990) is not possible. However, the ratio $\frac{I_{100}}{N(HI)}$ we find for the FIR ridges (~ 1.5 MJy ster $^{-1}$ /10 20 atoms cm $^{-2}$) is in the range of that measured for cirrus clouds. We determined N(HI)

from the brightness temperature using data from Fig. 9 and applying the conversion

$$N(HI) = 1.8 \cdot 10^{18} \int T_B(v) dv \quad (2)$$

assuming that the HI is optically thin.

The VR is located close to the northernmost point of the North Polar Spur (NPS) and could, in principle, be part of it. The NPS is presumably the remnant of a ~ 15 Myr old explosive event in the direction of the Galactic center, which released 10^{56} ergs and could be the outcome of $\sim 10^5$ supernovae produced in a small region within one million years. The giant loop is detected in a number of wavebands, from the X-ray to the radio continuum (Sofue 1994). The possibility that the VR is part of a small structure, extending to lower galactic longitudes from near the northernmost apex of the large NPS feature in Sofue's Fig. 2 (Plate L11), cannot be excluded.

It is also clear that the Virgo Ring (VR) is not a known high velocity cloud, because the compilation of Deul & van Woerden (1990) lists as nearest object HVC 2 at $12:09+15:32$ and $v_{lsr}=100.7 \text{ km s}^{-1}$, covering 3.2 square degrees of the sky. Wakker & van Woerden (1997) list a possible small HVC near the VR location. This is an HI feature associated with optical absorption lines observed in SN 1994D, located at $l=290^\circ.07$; $b=+70^\circ.13$ and $\sim 240 \text{ km s}^{-1}$ LSR. This SN occurred in NGC 4526, and the absorbing gas (with five absorption systems) was found by Ho & Filippenko (1996) at the same velocity as the HI measured by Kumar & Thonnard (1983). Ho & Filippenko mention other similar absorption features in the spectrum of SN 1991T (at $l=292.59$; $b=65.18$, in NGC 4527), which is $\sim 5^\circ$ away from SN1994D. It seems that there is material in the general direction of the VR with LSR velocities a few 100 km s^{-1} , and that it contains at least Ca II and Na I. In the vicinity of the VR, velocities in excess of 100 km s^{-1} are required in order to qualify an HI feature as a HVC.

Our analysis of the HI distribution and kinematics, using the LDS survey data, indicates that there is a significant disturbance of the hydrogen at the location of the VR. In particular, the three-peak structure of the velocity-column density is peculiar. There are a number of possible explanations for this HI peculiarity, starting from an expanding supernova (SN) shell, a collision

between Galactic HI and a high-velocity cloud, an ejection of a number of shells from a red (super)giant, etc. Each of these possibilities imposes some constraints on the problem.

Of all these possibilities, we consider the most likely to be that of a past collision between a small HI cloud and Galactic hydrogen. The HI remnant of this event could be the feature seen at -30 km s^{-1} in the high-FIR area and the Galactic HI would be the prevalent emission at -7 to -9 km s^{-1} , which shows up in all plots. At a velocity difference of $\sim 20 \text{ km s}^{-1}$ the collision would be highly supersonic. We note that the immediate vicinity of the VR has been studied in exactly this context by Stark *et al.* (1994). The region most likely to be part of the same complex is the BX field (see Table 1 of Stark *et al.* 1994), where the X feature peaks near -8 km s^{-1} (LSR) but there are parts of the B feature where velocities up to -40 km s^{-1} are observed.

Stark *et al.* (1994) interpreted the “intermediate negative velocity” (INV) gas, with $v \leq -20 \text{ km s}^{-1}$, as material at local velocity displaced by a shock following a collision with a high velocity cloud. The difference in LSR velocity between the BX features and candidate HVCs in this vicinity (at a few 100 km s^{-1} positive) forced Stark *et al.* to propose scenarios for the dissipation of the impinging HVC. They asserted that this cloud has evaporated and is now present as high-temperature gas. Collisions of HVCs with the Galactic disk have been studied by Kerp *et al.* (1996). They show that a collision with a differential velocity of 25 km s^{-1} may increase the temperature of the post-shock material from 10^4 to 10^5 K ; such temperatures are consistent with the EUVE measurements (Lieu *et al.* 1996).

It is possible to estimate the parameters of the Main Blob (MB) using the HI information from the LDSS. With the T_B value from -30 to -20 km s^{-1} we find

$$\langle N(\text{HI}) \rangle \approx 1.5 \cdot 10^{20} \text{ cm}^{-2} \quad (3)$$

This implies a gas-to-dust ratio for the MB of $\frac{N(\text{HI})}{E(B-V)} \approx 5 \cdot 10^{20} \text{ cm}^{-2} \text{ mag}^{-1}$, different from the canonical value for the Galaxy ($\frac{N(\text{HI})}{E(B-V)} = 5.4 \cdot 10^{21} \text{ cm}^{-2} \text{ mag}^{-1}$; Bohlin 1975). The MB appears, therefore, to be dust-rich (or HI-poor). Its projected angular size is $\sim 0^\circ.5$; this translates to a

size of $10(\frac{d}{1\text{kpc}})$ pc and a total hydrogen mass of

$$M_{\text{tot}}(\text{HI}) \approx 100 \frac{d}{1\text{kpc}} M_{\odot} \quad (4)$$

with an average (volume) density of $\sim 4(\frac{d}{1\text{kpc}})^{-1}$ cm $^{-3}$ assuming a spherical configuration. The cloudlet carries significant kinetic energy, considering its velocity relative to the Galactic HI (assumed to be ~ -9 km s $^{-1}$); $E_K \approx 3 \cdot 10^{47}(\frac{d}{1\text{kpc}})^2$ ergs. Also, the HI profile observed in its direction (see top panel of Fig. 9) is significantly wider than that of the second blob (bottom panel of Fig. 9). This could be an indication of higher turbulence within the MB relative to other HI entities in the same vicinity but at less negative LSR velocities.

It is significant that the MB, an infalling HI gas cloudlet, contains dust grains as evidenced by the extinction it produces. This indicates that any shocks that the material in MB might have encountered did not heat up its material to temperatures high enough to completely destroy the grains. However, its highly supersonic interaction with the ambient HI distribution caused a wider 21 cm profile. The MB produces significant extinction and is fairly distant from the MW plane while having an intermediate LSR velocity. This is different from the findings of Knude & Høg (1999), who concluded that intermediate-velocity HI clouds show no extinction.

The detection of HI condensations on sub-degree scales and high above the Galactic plane is relevant for the studies of galaxies in the Virgo cluster and beyond. A spectroscopic survey of objects in the background clusters at $z \approx 0.08$ could reveal absorption lines produced by material within the MB cloudlet. This, along with a measure of the ionization presumably taking place at the interface between the MB and the ambient HI, could reveal its composition and location. The essential finding is, however, the small scale on which significant extinction variations are encountered at high $|b|$. This shows that the derivation of “average extinction dependences”, *e.g.*, with galactic latitude (Knude 1996), is not very relevant to the determination of cosmologically-important parameters from studies of individual VC galaxies.

Our study shows that dust can affect the light of background galaxies in the VC and, through this, the determination of H_0 by using Cepheid photometry. This HST Key Project relies on a

canned approach to deredden individual stars and is based on the “standard” MW extinction law with $R = \frac{A_V}{E(B-V)} = 3.3$ (c.f. Madore & Freedman 1991). It remains to be proven that this relation applies for high galactic latitude dust clouds, such as those studied here.

4. Conclusions

We detected a dusty HI cloud seen in projection against the central regions of the Virgo cluster. We showed that the cloud, which appears ring-like in low-resolution FIR and total HI maps, has a complex FIR morphology when examined with higher resolution. The HI kinematics indicate a substantial disturbance at this location.

The Virgo Ring (VR) is located beyond the main body of the Galaxy, because the distributions and colors of stars in its direction are not affected by it. The cloud could not be more distant than the VC, because it influences the colors of galaxies within the cluster. The HI evidence argues strongly for a relatively nearby location. The connection of the ring with the North Galactic Spur may be accidental, but the peculiar morphology and kinematics of the HI associated with the FIR emission make a connection, perhaps through a collision between an HI cloud and Galactic HI, more likely. Such a collision could perhaps explain also the extreme-UV (or soft X-ray) emission observed from the neighborhood of M87.

The importance of our finding lies in the possibility that many key observations done in the direction of the Virgo cluster may have been adversely affected by extinguishing clouds, which are not homogeneous and where the total V-band extinction may reach up to a few tenths of a magnitude.

Acknowledgements

NB acknowledges support from the Israel Science Foundation. EA is supported by a grant from the Israel Ministry of Science to develop TAUVE, a UV imaging telescope. KR and BW

were supported by the Polish KBN grant number C76/98. We are grateful to Drs. C.K. Young and M.J. Currie for supplying electronic versions of the VPC data tables in advance of publication. NB is grateful to Mike Hauser for discussions on the reality of COBE/DIRBE features, to John Bahcall for allowing public use of his Galaxy model, and to Sara Beck and Sasha Kashlinsky for critical readings of one of the first drafts.

Appendix

Classical Wolf diagrams for galaxies (*e.g.*, Zonn & Rudnicki 1965) were made for the regions labelled A through D in Fig. 4 and are shown in Figure 5. Only curve C could be interpreted as shaped by extinction, and this only by a large amount of leeway. Curve A, as already cautioned, has a completely different shape. Both A and D curves are higher than the comparison curve B, and are presumably shaped by the inhomogeneous distribution of galaxies in the VC area. If, however, we would adopt curve C as representative for the background galaxies (no VC subclusters or background galaxy clusters are evident in this area), then the obscuring cloud would have to be relatively nearby, as no parts of the C and B curves overlap.

To prevent distortion of the results by possible subclustering, we decided to study the color distribution of the background galaxies. The advantage of using color is that this parameter is distance-independent, provided the objects of study are not “too distant”, in the sense of requiring a k-correction. We assume that the objects in the VPC conform to this constraint and do not attempt to correct the color for redshift (which is not known, in most cases). We also caution about “edge effects”, which could arise because of a smaller population of the sub-areas located near the edges of the VPC coverage; such areas cover less than one square degree, have less than the average number of galaxies, and would be less representative.

We analyzed the color distribution of all galaxies in the entire VPC. We selected objects only by their position; specifically, we included all the objects listed in the catalog with their magnitudes and colors, without separating them by morphological type, apparent blue magnitude,

angular size, being members or non-members of the cluster, etc. The area enclosed within $184^\circ < \alpha < 189^\circ$ and $10^\circ < \delta < 16^\circ$ was divided into square degree areas at integer α and δ values. In each sub-area we calculated the statistics of the color distribution for the galaxies. The total number of galaxies per cell does not appear to show a specific pattern, apart for the edge effects mentioned above.

We checked the distribution of photometric indices over the sub-areas of the VPC against the locations of the enhanced FIR emission. In each one square degree area we counted the galaxies, calculated their mean B_J magnitude and the average $(U-B_J)$, (B_J-R_C) , and $(U-R_C)$ color indices, and studied the statistical properties of the distributions of the color indices in each area. The color index $(U-R_C)$ has been calculated as $(U-B_J)-(B_J-R_C)$. The results are presented in Tables A1 and A2 for $(U-R_C)$, where each cell contains these parameters for each one square degree region. The results for the other color indices were similar and are not shown.

Each sub-area in Table A1 is represented by one cell in the table, where the rows are the declination of the sub-areas and the columns are the right ascension, both in decimal degrees. The distribution of the $(U-R_C)$ color is represented by the mean, the standard error of the mean (in round brackets), and the number of galaxies in the sub-area [in square brackets]. The standard error of the mean SE_a is defined as:

$$SE_a = \frac{SD_a}{\sqrt{N_a}} \quad (5)$$

Here SD_a is the standard deviation of the values in sub-area a , and N_a is the number of galaxies in the same sub-area.

Table A2 shows the properties of the distribution of $(U-R_C)$ in each of the one square degree areas. Specifically, we list the kurtosis with its standard error, and the skewness with its standard error, for the distribution of galaxies within the square degree area. These are listed in order to demonstrate how much are the distributions of $(U-R_C)$ values in individual cells similar (or different).

The significance of possible differences among the cells was considered using the mean and its

standard error. A Student's *t-test* between the means, by which one estimates the variable

$$t = \frac{|\langle X_1 \rangle - \langle X_2 \rangle|}{\sqrt{SE_1^2 + SE_2^2}} \quad (6)$$

was performed. Here $\langle X_i \rangle$ is the mean of variable i , and SE_i is its standard error of the mean (e.g., Brandt 1970).

A cursory perusal of Table A1 shows that the only sub-areas where $(U-R_C)$ is small, and which are not on the borders of the VPC (Currie & Young 1998), are the two areas at $(\alpha=187.5, \delta=13.5)$, which we call “area GA”, and at $(187.5, 14.5)$ which we call “area GB”. These regions are central in the Virgo Ring (VR) and this finding, if significant, could indicate less wavelength-dependent extinction in this direction (which shows reduced FIR emission) than in neighboring areas. The comparison is done with two regions located in the direction of enhanced FIR emission, at $(186.5, 12.5)$ which we call “area GC”, and at $(188.5, 12.5)$ which we call “area GD”. The latter area is located at the edge of the VPC but does not appear to be depleted in galaxies, thus the comparison with it is valid.

Using the t-test described above, the difference in means of the $(U-R_C)$ color index between areas GA and GC yields $t=1.97$ (significant at the 95% level), and between areas GA and GD $t=2.72$ (significant at the 99.5% level). A similar significance level was found for the difference between areas GB and GC, with $t=2.76$. The results of the t-test indicate that the galaxies in the VPC, which are located behind the low FIR emission area, are slightly bluer than others which are located behind areas of high FIR emission. This impression is supported by an examination of the higher moments of the distribution (Table A2). The skewness of the $(U-R_C)$ values in areas GA and GB is very similar, but is very different from the skewness of the distribution in areas GC and GD.

References

Abadi, H.J. & Edmunds, M.G. 1978, A&A, 70, 189

Almoznino, E. & Brosch, N. 1998, MNRAS, 298, 920

Bahcall, J.N. & Soneira, R. 1984, ApJS, 55, 67

Beichman, C.A., Neugebauer, G., Habing, H.J., Clegg, P.E. & Chester, T.J. 1988 *IRAS Catalogs and Atlases: Vol. 1 (Explanatory Supplement)*, NASA RP-1190

Binggeli, B., Sandage, A. & Tammann, G.A. 1985, AJ, 90, 1681

Blitz, L., Spergel, D.N., Teuben, P.J. & Hartmann, D. 1999, astro-ph/9901307

Bohlin, R.C. 1975, ApJ, 200, 402

Böhringer, H., Nulsen, P.E.J., Braun, R. & Fabian, A.C. 1995, MNRAS, 274, L67

Böhringer, H., Briel, U.G., Schwarz, A., Voges, V., Hartner, G. & Trumper, J. 1994, Nature, 368, 828

Bothun, G., Impey, C.D., Malin, D.F. & Mould, J.R. 1987, AJ, 94, 23

Bothun, G., Schombert, J.M., Impey, C.D. & Schneider, S.E. 1990, ApJ, 360, 427

Brandt, S. 1970 *Statistical and Computational Methods in Data Analysis*, Amsterdam: North-Holland Publishing Co., pp. 125 *et seq.*

Currie, C.K. & Young, M.J. 1998, A&AS, 127, 367

de Blok, W.J.G. 1997, PhD thesis, University of Groningen

de Blok, W.J.G., van der Hulst, J.M. & Bothun, G.D. 1995, MNRAS, 274, 235

Deul, F.R. & Burton, W.B. 1990, A&A, 230, 153

Egger, R.J. & Aschenbach, B. 1995, A&A, 294, L25

Ferguson, H.C. 1993, MNRAS, 263, 343

Ferguson, H.C., Tanvir, N.R. & von Hippel, T. 1998, Nature, 391, 461

Giovanelli, R. & Haynes, M. 1989, ApJ, 346, L5

Graham, J.A., Ferrarese, L., Freedman, W.L. *et al.* 1998, BAAS, 192, 66.12

Haikala, L.K., Mattila, K., Bowyer, S., Sasseen, T.P., Lampton, M. & Knude, J. 1995, ApJ, 443, L33

Hartmann, D. & Burton, W.B. 1997, *Atlas of Galactic Neutral Hydrogen*, Cambridge (UK): Cambridge University Press

Hauser, M.G., Kelsall, T., Leisawitz, D. & Weiland, J. 1997, *COBE Diffuse Infrared Background Experiment (DIRBE) Explanatory Supplement*, COBE Reference Document Ref.No. 97A

Heller, A., Almoznino, E. & Brosch, N. 1998, MNRAS, in press

Ho, L.C. & Filippenko, A.V. 1996, ApJ, 463, 818

Hoffmeister, C. 1962, Z.f.Astrophys., 55, 40

Kashlinsky, A. 1999, private communication

Katsiyannis, A.C., Kemp, S.N., Berry, D.S. & Meaburn, J. 1998, A&AS, 132, 387

Kerp, J., Mack, K.-H., Egger, R., Pietz, J., Zimmer, F., Mebold, U., Burton, W.B. & Hartmann, D. 1996, A&A, 312, 67

Knude, J. & Høg, E. 1999, A&A, 341, 451

Knude, J. 1996, A&A, 306, 108

Kumar, K.C. & Thonnard, N. 1983, AJ, 88, 260

Lagache, G., Abergel, A., Boulanger, F. & Puget, J.-L. 1998, A&A, 333, 709

Leggett, S.K., Clowes, R.G., Kalafi, M., MacGillivray, H.T., Puxley, P.J., Savage, A. & Wolstencroft, R.D. 1987, MNRAS, 227, 563

Lieu, R., Mittaz, J.P.D., Bowyer, S., Lockman, F.J., Hwang, C.-Y. & Schmitt, J.H.M.M. 1996, ApJL, 458, 5

Lo, K.Y. & Sargent, W.L.W. 1979, ApJ, 227, 756

Macri, L.M. *et al.* 1999, astro-ph/9901332

Madore, B. & Freedman, W.L. 1991, PASP, 103, 933

Maoz, D. 1995, ApJ, 455, L115

Murawski, W. 1983, Acta Cosmologica, 12, 7

Okroy, R. 1965, Astron. Cirk., 320, 4

Pickering, T.E., Impey, C.D., Van Gorkom, J.H. & Bothun, G.D. 1997, AJ, 114, 1858

Rudnicki, K. 1986, *Gamov Cosmology* (F.Melchiorri & R.Ruffini, eds.), LXXXVI Corso of the Soc. It. Fisica, Bologna, p. 480

Rudnicki, K. & Baranowska, M. 1966, Acta Astron., 16, 65

Schneider, S.E., Helou, G., Salpeter, E.E. & Terzian, Y. 1983, ApJ, 273, L1

Schlegel, D.J., Finkbeiner, D.P. & Davis, M. 1998, ApJ, 500, 525

Sofue, Y. 1994, ApJ, 431, L91

Sprayberry, D., Impey, C.D., Irwin, M.J., McMahon, R.G. & Bothun, G.D. 1993, ApJ, 417, 114

Stark, R., Dickey, J.M., Burton, W.B. & Wennmacher, A. 1994, A&A, 281, 199

Taylor, C.L., Thomas, D.L., Brinks, E. & Skillman, E.D. 1996, ApJS, 107, 143

van den Bergh, S. 1996, PASP, 108, 1091

Wakker, B.P. & Boulanger, F. 1986, A&A, 170, 84

Wakker, B.P. & van Woerden, H. 1991, A&A, 250, 509

Wakker, B.P. & van Woerden, H. 1997, ARAA, 35, 217

Weil, M.L., Bland-Hawthorn, J. & Malin, D.F. 1997, ApJ, 490, 664

Wszolek, B., Rudnicki, K., de Bernardis, P., Masi, S. & Salvi, A. 1988a, Ap.Space Sci. 152, 29

Wszolek, B., Rudnicki, K., de Bernardis, P. & Masi, S. 1988b, in *Large Scale Structures in the Universe*, (Seitter, W.C., Duerbeck, H.W. & Tacke, M., eds.) Lecture Notes in Physics 310, 223

Wszolek, B., Rudnicki, K., de Bernardis, P. & Masi, S. 1989, *The World of Galaxies* (Corvin, H.G., Jr. & Bottinelli, C., eds.) p. 499

Zonn, W. 1957, Bull. Acad. Polonaise des Sciences, vol. V, no. 1, 47

Zonn, W. & Stodolkiewicz, J. 1958, Bull. Acad. Polonaise des Sciences, ser. sci. math. astr. phys. vol. VI, no. 3, 185

Zonn, W. & Rudnicki, K., 1965, in *Stellar Astronomy*, Washington DC, 168

Figure captions

Figure 1: FIR maps of the VR region. The top right panel shows the IRAS $100\mu\text{m}$ map. The COBE/DIRBE $100\mu\text{m}$ (top left panel) and $240\mu\text{m}$ emission (lower left panel) show the VR, but have a lower angular resolution than the IRAS $100\mu\text{m}$ map. The contours of the FIR emission are in MJy ster^{-1} . For orientation purposes, the location of M87 is (187.07, +12.67).

Figure 2: Wolf diagram for USNO-A2.0 stars in five selected regions, one corresponding to the lowest FIR-emitting region in Fig. 1 and the other four coinciding with peaks of the FIR emission. The regions are defined in Table 1 and the cumulative distributions are depicted as follows: USNO1222+1330 as a dotted line, USNO1226+1430 as a dashed line, USNO1230+1130 as a long-dashed line, USNO1230+1330 as a solid line with open squares, and USNO1234+1230 as a dot-dashed line.

Figure 3: Comparison of predicted star counts (using the Bahcall-Soneira model) and the actual star counts from the USNO-A2.0 catalog, for the five regions listed in Table 3. Each region is one degree square; the actual star counts are represented by open squares and the model prediction is shown as the solid line.

Figure 4: Selected areas to check for total extinction effects on galaxies. The contours refer to the IRAS $100\mu\text{m}$ map and the heavy-lined parallelograms marked A through D are the selected areas for testing the number density of galaxies.

Figure 5: Wolf diagram for galaxies. The three distribution curves A, C, D correspond to regions within higher FIR emission of Fig. 1 and curve B to the region of low FIR emission. For explanation of the designations A, B, C, D see Fig. 5. The data from each of the regions is depicted as follows: region A - solid line, region B - dotted line, region C - dashed line, and region D - long-dashed line.

Figure 6: Total HI column density from the LDS (left panel) compared with the IRAS $100\mu\text{m}$

emission (right panel). Darker shades in the HI plot correspond to higher column densities. Lighter shades in the FIR plot correspond to more intense emission.

Figure 7: Galactic latitude-velocity plots near $b \approx 75^\circ$ for $l=276.0$ (top panel), $l=283.0$ (middle panel), and $l=290.5$ (bottom panel). The first plot corresponds to the main blob (more intense FIR emission), the second to the “hole”, *i.e.*, center of the VR, and the third to the second blob (next intense FIR emission). The horizontal band marked with heavy lines in each panel indicates the region for which data were used to plot Fig. 8.

Figure 8: Cuts through the position-velocity plots of Fig. 7, averaging the brightness temperature for $b=74^\circ$, $74^\circ.5$, and $b=75^\circ$ (three latitude bands). The order of the plots is like in Fig. 8. The average HI column density shows the velocity distribution of HI clouds in this region. Three peaks stand out clearly, with the most intense one at the highest negative velocities for the main blob.

Table 1. Regions for testing stellar properties

Name	Center(1950)	Center(degrees)	(l, b)	N_{stars}
USNO1222+1330	12:22:00 +13:30:00	185.5 +13.5	277.3 +74.7	1804
USNO1226+1430	12:26:00 +14:30:00	186.5 +14.5	279.3 +76.0	1593
USNO1230+1130	12:30:00 +11:30:00	187.5 +11.5	286.4 +73.5	2126
USNO1230+1330	12:30:00 +13:30:00	187.5 +13.5	284.4 +75.4	1696
USNO1234+1230	12:34:00 +12:30:00	188.5 +12.5	289.0 +74.7	1669

Note. — Each region is a one degree square centered on the listed coordinates. The stars were extracted automatically from the USNO-A2.0 catalog.

Table 2. A1: Photometric properties of VPC galaxies ($U-R_C$)

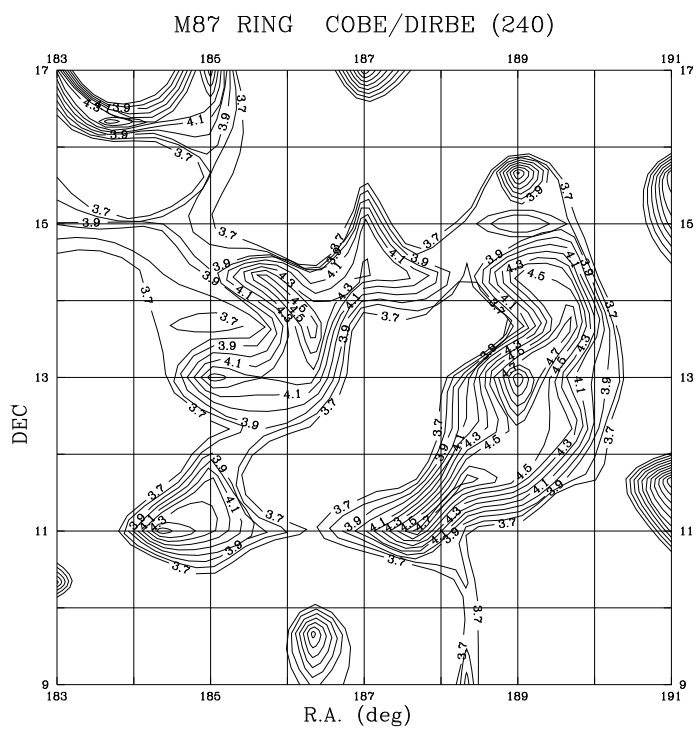
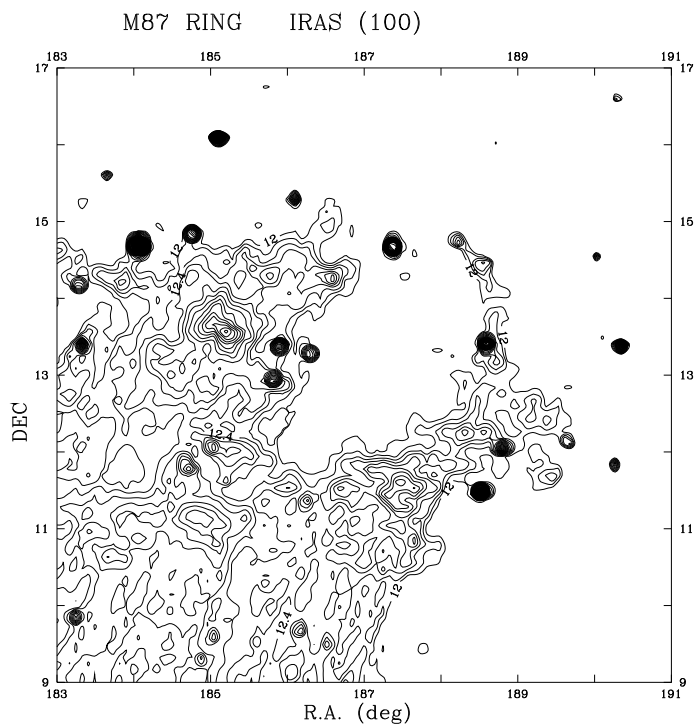
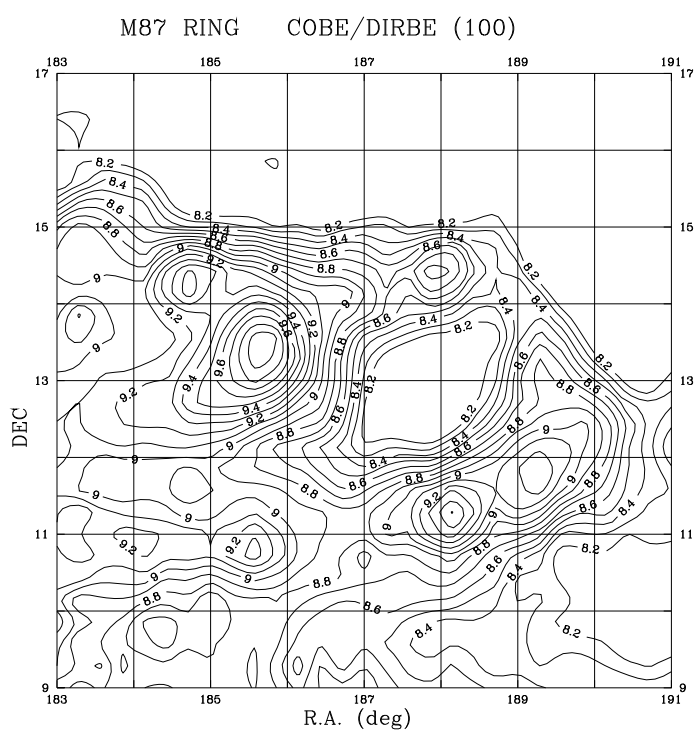
δ/α	184.5	185.5	186.5	187.5	188.5
15.5	1.485(.109)[08]	1.300(.103)[04]	1.360(.186)[06]	1.678(.162)[08]	1.751(.118)[12]
14.5	1.347(.079)[27]	1.476(.060)[48]	1.547(.061)[46]	1.380(.096)[26]	1.526(.083)[30]
13.5	1.573(.053)[68]	1.508(.057)[56]	1.545(.074)[39]	1.390(.094)[26]	1.445(.090)[22]
12.5	1.363(.070)[36]	1.602(.047)[57]	1.608(.058)[51]	1.593(.070)[45]	1.693(.060)[35]
11.5	1.274(.075)[36]	1.582(.068)[32]	1.658(.054)[72]	1.514(.066)[45]	1.420(.101)[26]
10.5	1.296(.070)[11]	1.347(.077)[22]	1.530(.099)[23]	1.596(.104)[20]	1.054(.114)[14]

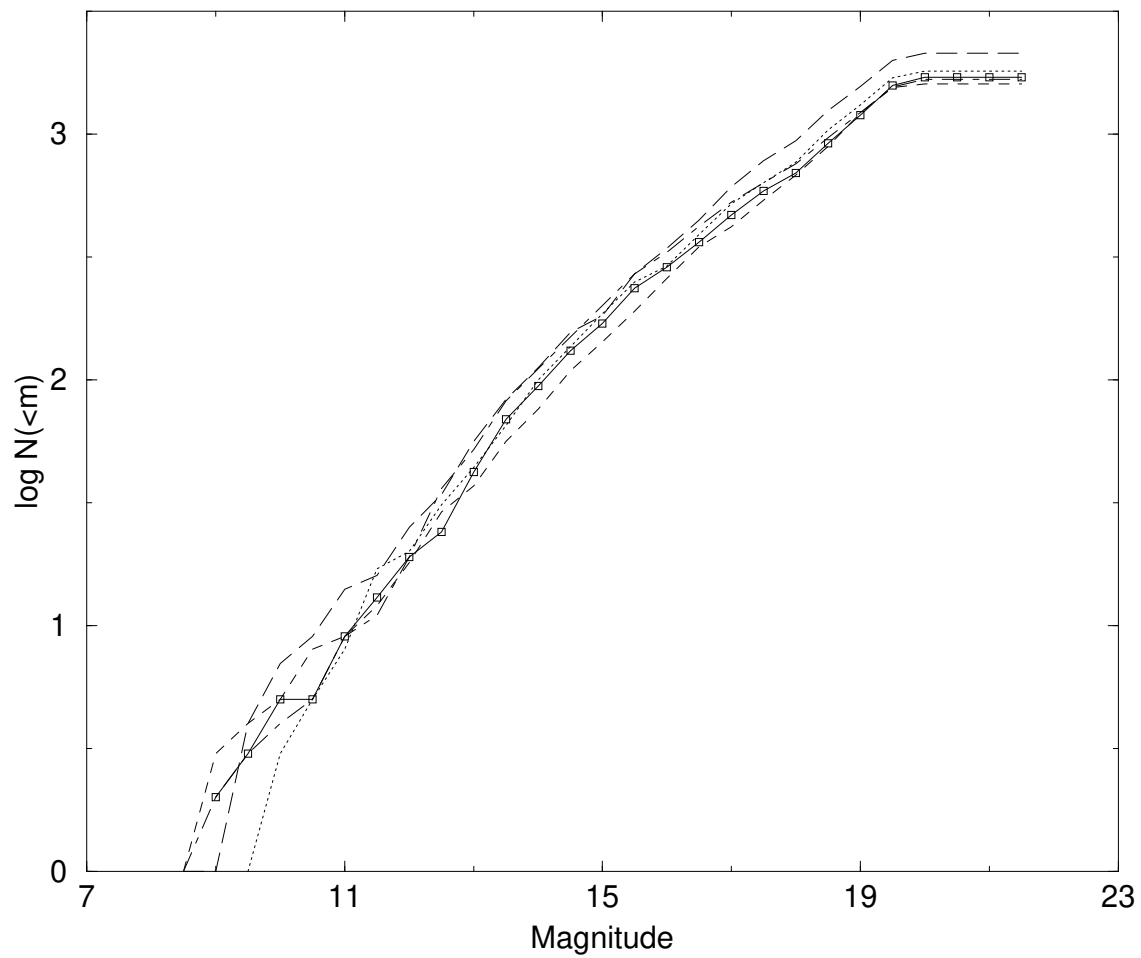
Note. — Each cell in the table contains the average ($U-R_C$) color index, the standard error of the mean (in round brackets), and the number of galaxies in area cell [in square brackets]. The cells, except those at the edges of the VPC coverage which are smaller, are labeled by their central (α , δ) coordinates, which are given in decimal degrees.

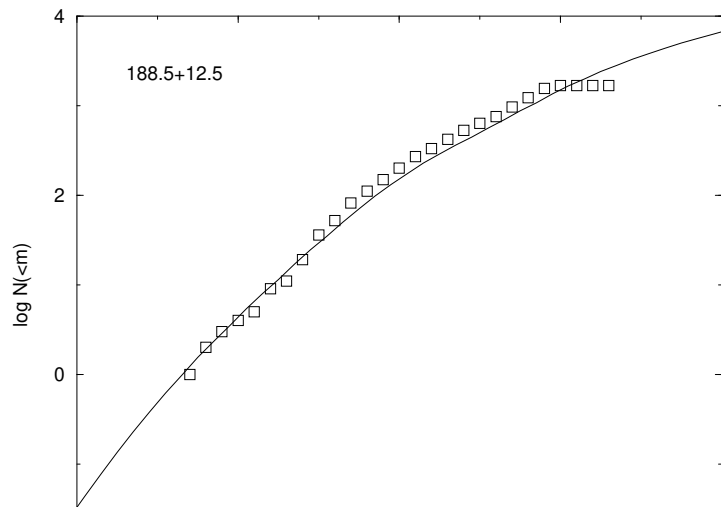
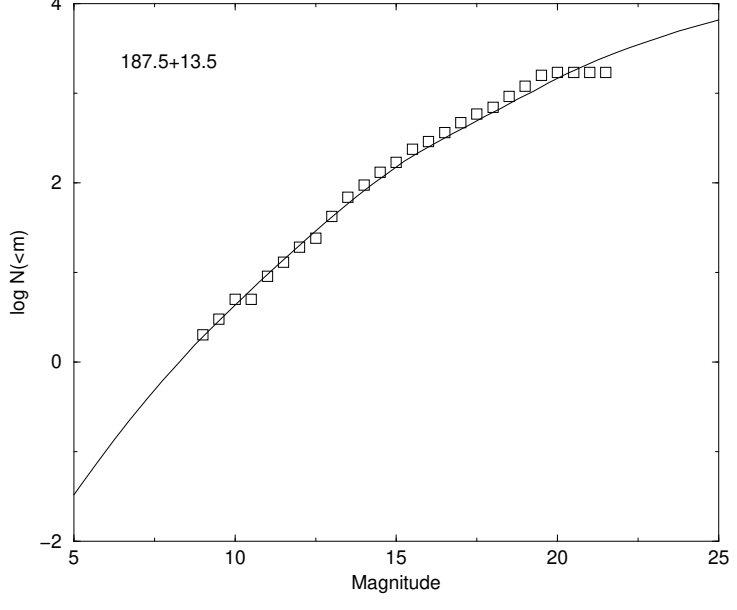
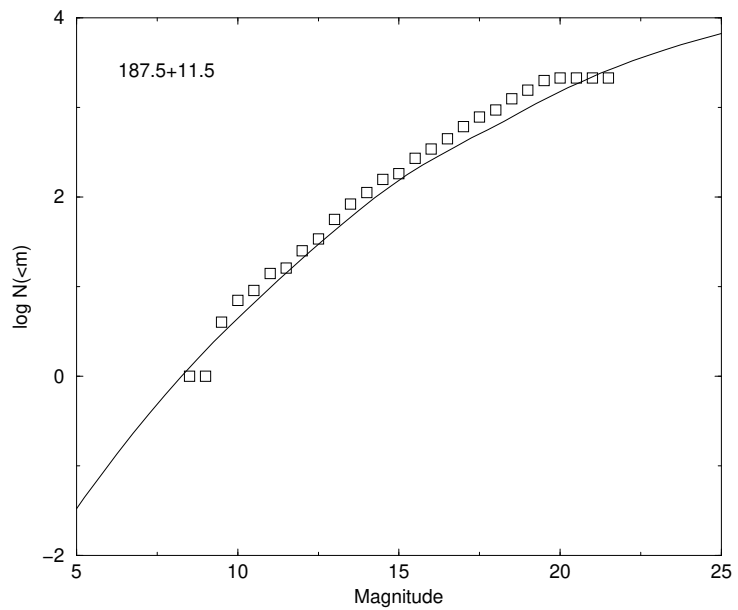
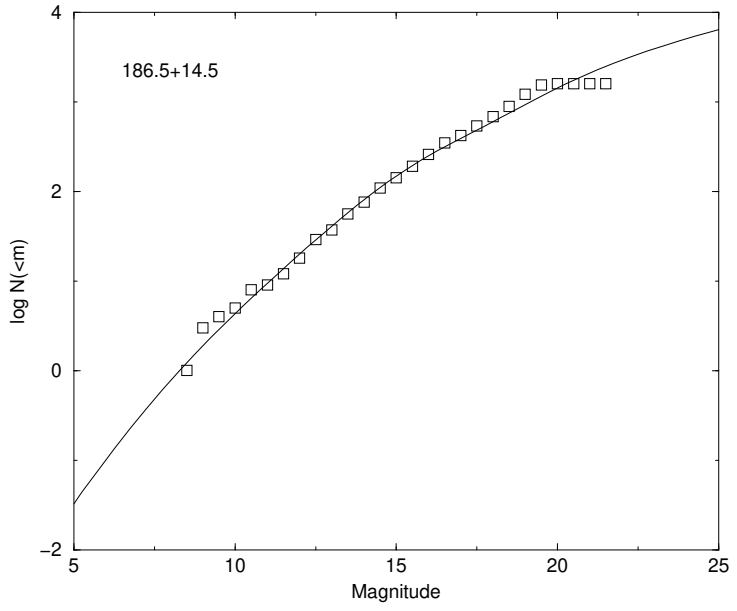
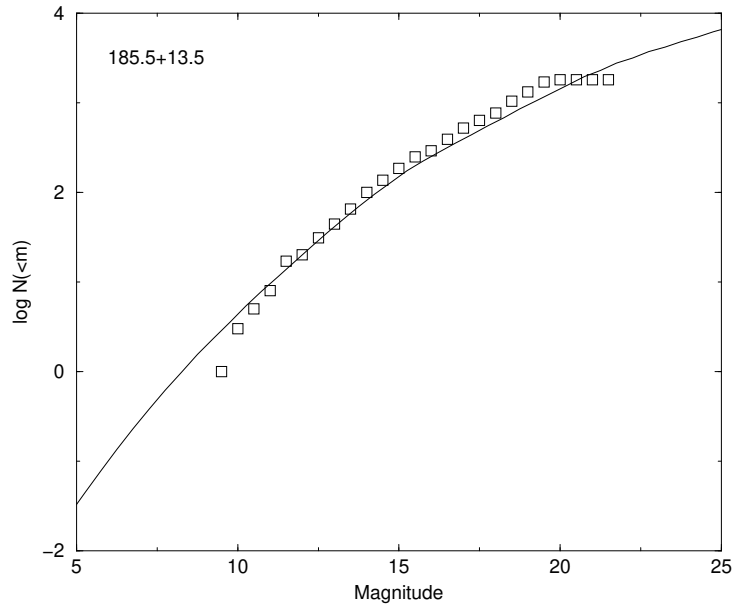
Table 3. A3: Statistical distribution properties of $(U-R_C)$ in VPC galaxies

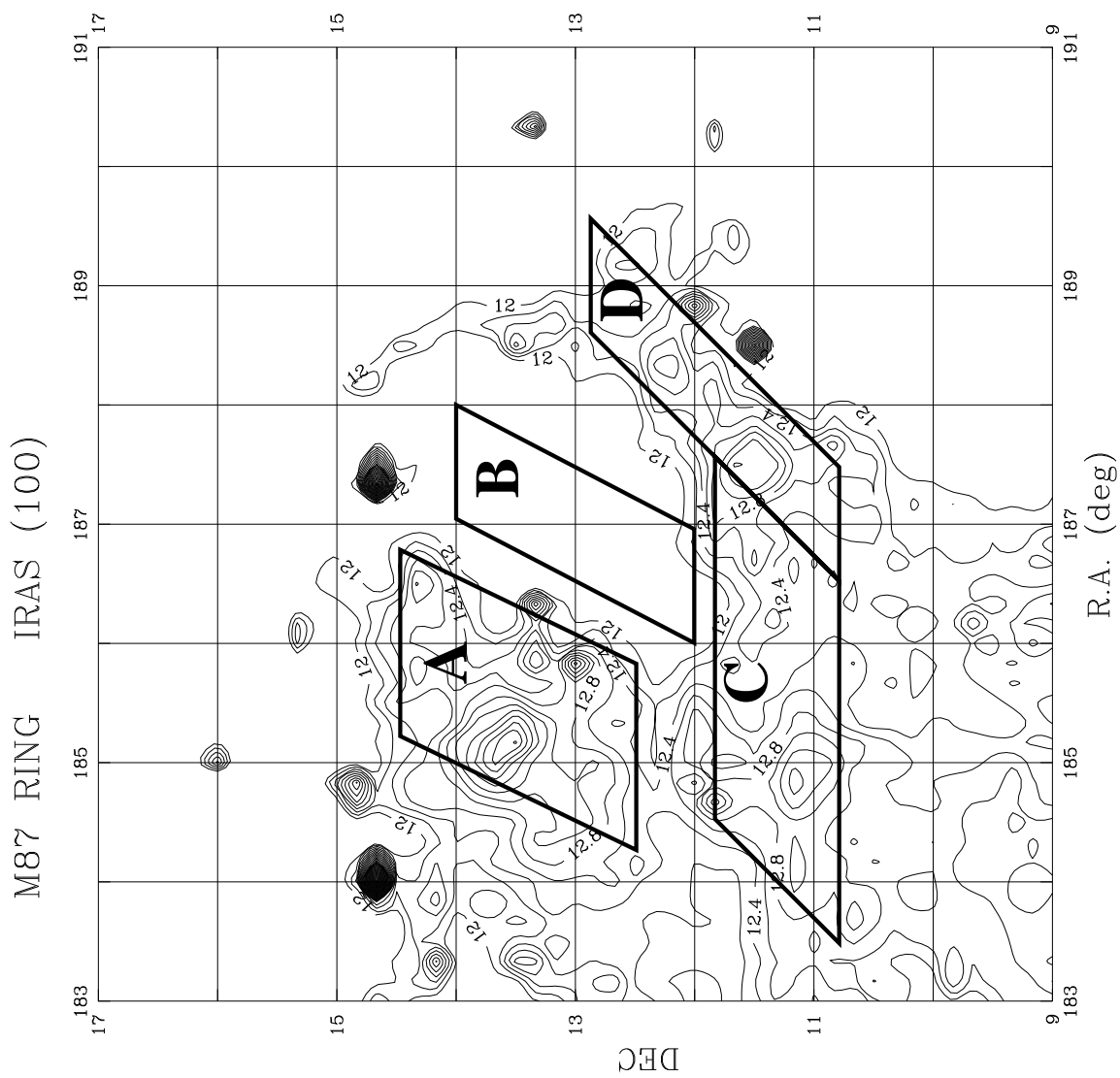
δ/α	184.5	185.5	186.5	187.5	188.5
15.5	-.37(1.48) .11(.75)	1.89(2.62) 1.35(1.01)	.83(1.74) .16(.85)	.74(1.48) -.46(.75)	.18(1.23) -.64(.64)
14.5	-.31(.87) .58(.45)	-1.38(.67) -.05(.34)	-1.10(.69) -.36(.35)	-.96(.89) .11(.46)	.35(.83) .00(.43)
13.5	.83(.57) -.86(.29)	-.32(.63) -.07(.32)	-.03(.74) .45(.38)	-.09(.89) .53(.47)	1.89(.95) -.91(.49)
12.5	-.43(.77) -.33(.39)	1.38(.62) -.71(.32)	.43(.67) -.47(.33)	.35(.70) -.64(.35)	-.93(.78) -.43(.40)
11.5	-.47(.77) -.08(.39)	-1.06(.81) .10(.41)	-.21(.56) -.10(.28)	-.10(.70) .38(.35)	-.86(.89) -.02(.46)
10.5	.59(1.28) -.56(.66)	-1.04(.95) -.55(.49)	-.58(.94) -.55(.48)	.14(.99) .57(.51)	-.41(1.15) .11(.60)

Note. — Each cell contains the kurtosis and its standard error, and the skewness and its standard error, for the distribution of the $(U-R_C)$ color indices in each cell area. The errors for each statistical estimator are given in round brackets.



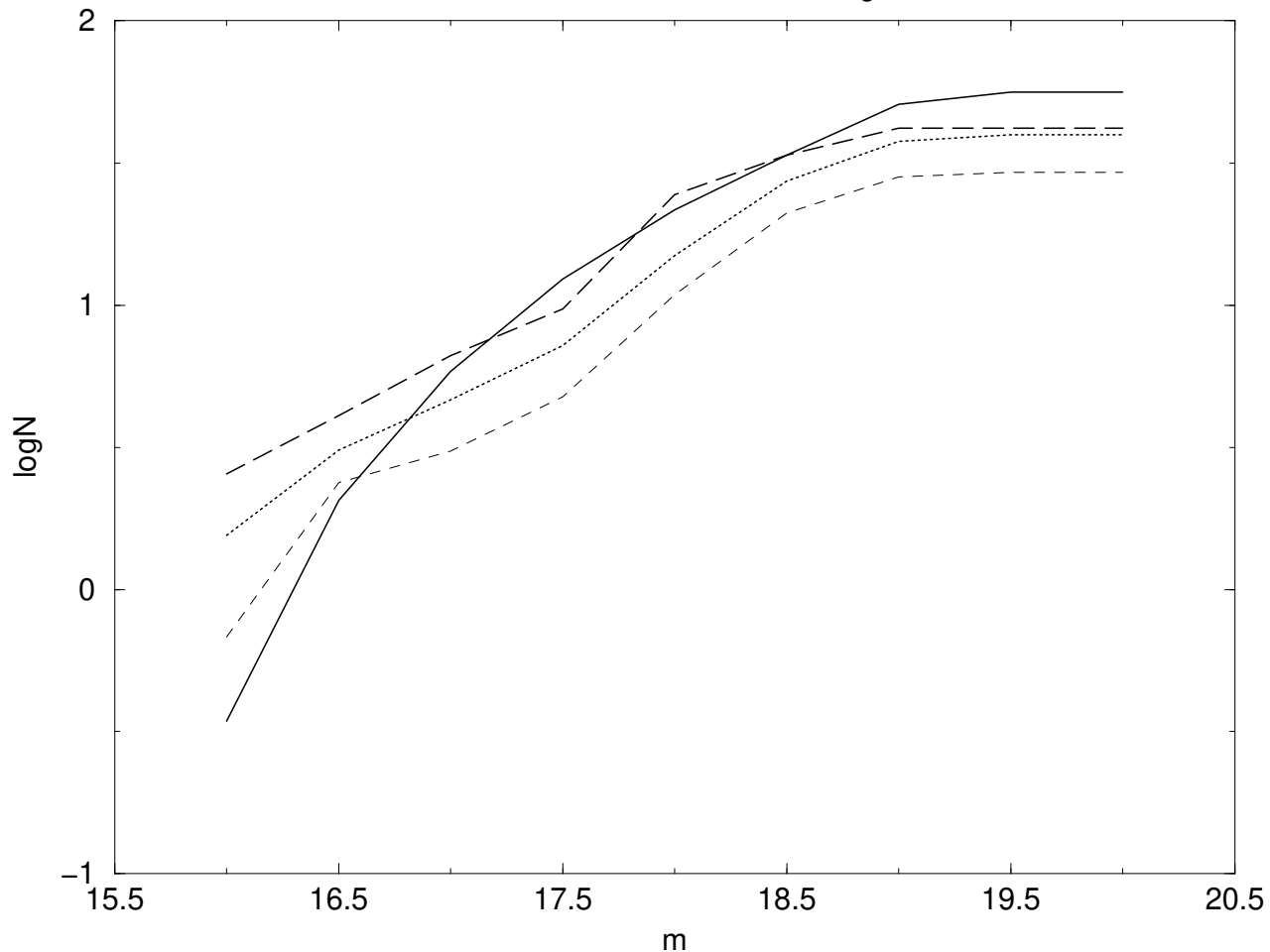


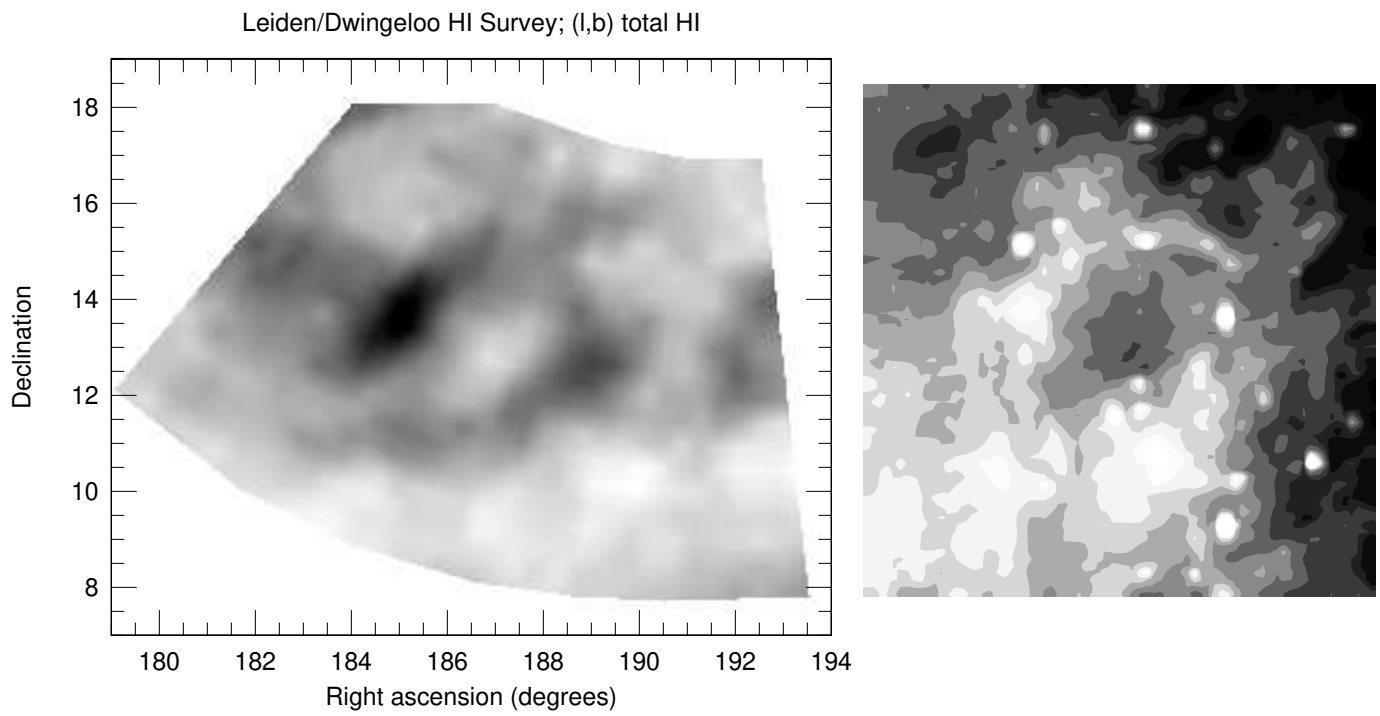




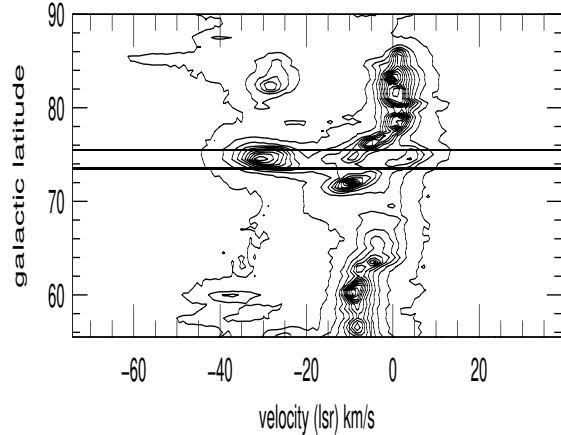
Wolf diagrams (M87–ring)

A–solid, B–dotted, C–dashed, D–long dashed

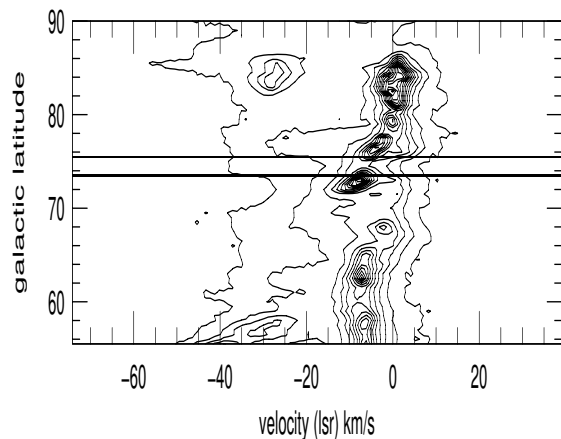




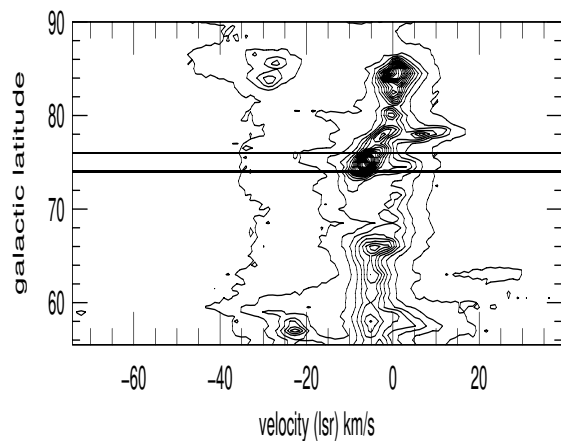
Leiden/Dwingeloo HI Survey; (b,v) at $l=276.0$

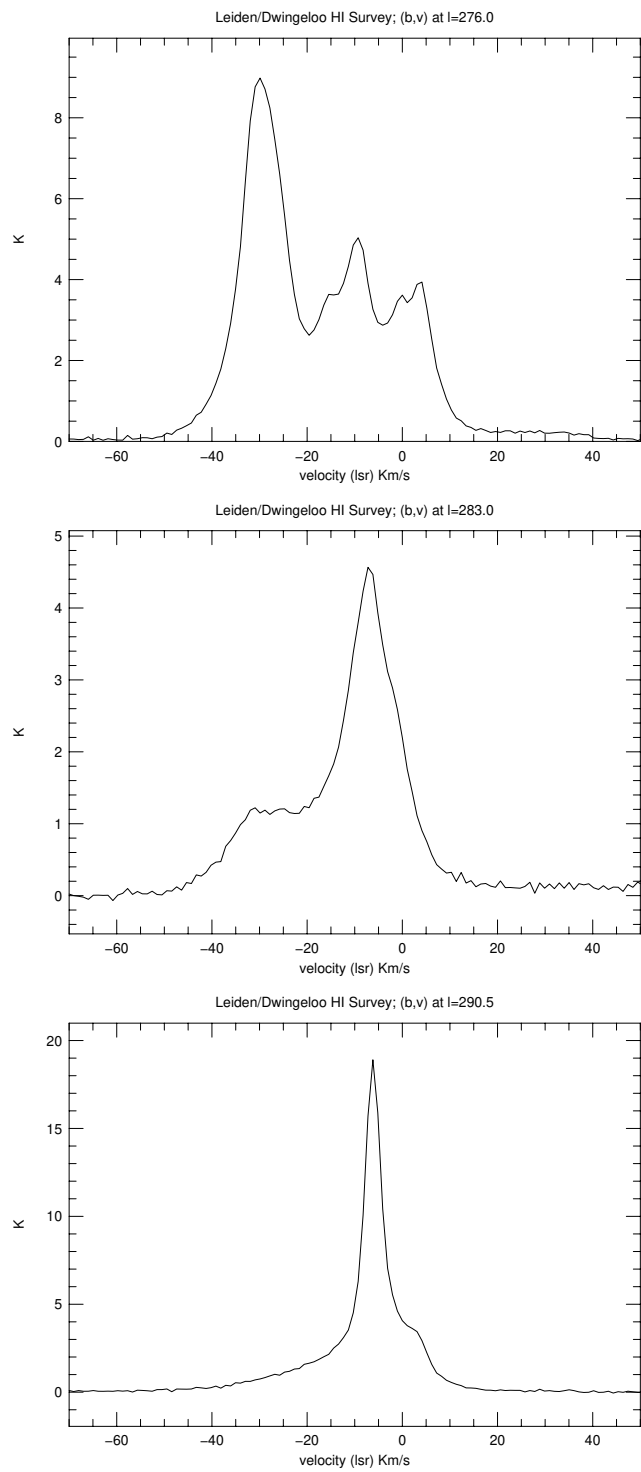


Leiden/Dwingeloo HI Survey; (b,v) at $l=283.0$



Leiden/Dwingeloo HI Survey; (b,v) at $l=290.5$





M87 RING IRAS (100)

